

Detailed Modeling of the Molecular Growth Process in Aromatic and Aliphatic Premixed Flames

A. D'Anna*

Dipartimento di Ingegneria Chimica, Università di Napoli "Federico II", Napoli, Italy

A. Violi

*Department of Chemical Engineering, University of Utah,
Salt Lake City, Utah 84112-1114*

Received January 28, 2004. Revised Manuscript Received July 21, 2004

A detailed kinetic model has been developed and used to simulate aromatic growth in premixed benzene and ethylene flames. The model considers the role of resonantly stabilized radicals in the growth of aromatic species, in addition to the hydrogen abstraction carbon addition (HACA) mechanism, which involves hydrogen abstraction to activate aromatics followed by subsequent acetylene addition. Model results show that the self-combination of resonantly stabilized radicals—in particular, the combination of cyclopentadienyl radicals—is the controlling pathway for the aromatic-ring growth. The kinetic model reproduces the experimental trends of these compounds already below the flame front and their decrease within the flame front, which has been observed experimentally but never predicted numerically. The reaction mechanism has been used to identify the different behaviors of aromatic growth in ethylene and benzene flames. Benzene formation is the rate-limiting step for aromatic growth in ethylene flames. C_6H_6 is formed across the flame front and carbon growth continues through the formation of multi-ring aromatics in the post-flame region. In benzene oxidation, the aromatic ring is already present in the main oxidation zone and it is mainly oxidized to cyclopentadienyl radicals. As a consequence, a large amount of cyclopentadienyl radicals are available for recombination reactions, leading to multi-ring formation already in the main oxidation region. The increase of the temperature at the flame front reduces their concentration due to pyrolysis and/or oxidation resulting in a peak value in the main oxidation region and a leveling-off in the post-oxidation region of the flame.

Introduction

In combustion systems, inadequate mixing of fuel and oxygen produces fuel-rich “pockets”, where incomplete oxidation results in carbon growth, starting with small radicals, going through the formation of aromatic species and ending up with soot particles. Control of these combustion-generated pollutants can be achieved through suppression of their formation, through enhancement of burnout after they are formed, or through a combination of these approaches.

To determine the proper combustion modifications to reduce pollutant emissions, it is important to know the controlling features of their formation mechanisms. Hence, an understanding of the elementary reaction pathways of hydrocarbon oxidation and pyrolysis and the growth of aromatic compounds is an area of interest, from both a fundamental combustion standpoint and an environmental standpoint.

The rich combustion of hydrocarbons is often characterized by the formation of a large variety of compounds, which constitute the emitted carbonaceous aerosol, including soot, polycyclic aromatic hydrocarbons

(PAH), high-molecular-mass tarlike material, and fullerenes.^{1–5} So far, efforts to model the complex chemistry of fuel-rich combustion have focused on the prediction of soot and low-molecular-mass PAH,^{6–12} which are not the major constituents of combustion-generated pollutants. Indeed, high-molecular-mass com-

(1) D'Alessio, A.; D'Anna, A.; D'Orsi, A.; Minutolo, P.; Barbella, R.; Ciajolo, A. *Proc. Combust. Inst.* **1992**, *24*, 973.

(2) McKinnon, J. Th. Chemical and Physical Mechanisms of Soot Formation, Ph.D. Thesis, Massachusetts Institute of Technology, Cambridge, MA, 1989.

(3) Ciajolo, A.; D'Anna, A.; Barbella, R.; Tregrossi, A. *Proc. Combust. Inst.* **1994**, *25*, 678.

(4) Grieco, W. J.; Lafleur, A. L.; Swallow, K. C.; Richter, H.; Taghizadeh, K.; Howard, J. B. *Proc. Combust. Inst.* **1998**, *27*, 1669.

(5) D'Alessio, A.; D'Anna, A.; Gambi, G.; Minutolo, P. *J. Aerosol Sci.* **1998**, *29* (4), 397–409.

(6) Frenklach, M.; Clary, D. W.; Gardiner, W. C. Jr.; Stein, S. E. *Proc. Combust. Inst.* **1985**, *20*, 887.

(7) Frenklach, M.; Warnatz, J. *Combust. Sci. Technol.* **1987**, *51*, 265–283.

(8) Frenklach, M.; Wang, H. Detailed Mechanism and Modeling of Soot Particle Formation. In *Soot Formation in Combustion*; Bockhorn, H., Ed.; Springer-Verlag: Heidelberg, Germany, 1994; pp 165–192.

(9) Wang, H.; Frenklach, M. *Combust. Flame* **1997**, *110* (1–2), 173–221.

(10) Castaldi, M. J.; Marinov, N. M.; Melius, C. F.; Huang, J.; Senkan, S. M.; Pitz, W. J.; Westbrook, C. K. *Proc. Combust. Inst.* **1996**, *26*, 693.

(11) Marinov, N. M.; Pitz, W. J.; Westbrook, C. K.; Castaldi, M. J.; Senkan, S. M. *Combust. Sci. Technol.* **1996**, *116–117*, 211–287.

(12) Richter, H.; Grieco, W. J.; Howard, J. B. *Combust. Flame* **1999**, *119* (1–2), 1–22.

* Author to whom correspondence should be addressed. Telephone: +39 081 768 2240. Fax: +39 081 593 6936. E-mail address: andrea.danna@unina.it.

pounds represent the largest fraction of the aromatics compounds in slightly sooting conditions and they remain almost unresolved in the analyses of combustion exhausts, as well as in the atmosphere.^{3,13–15}

Recently, we have developed a kinetic model for aromatic growth,^{16,17} which reproduces quite well the formation of total aromatic compounds (soot + high-molecular-mass structures) in rich flames of ethylene in a wide range of operating conditions. The amount and net rate of two- and three-ring aromatics predicted by the model agrees with the experimentally determined concentration and formation rates of soot and high-molecular-mass structures.

The model also replicates the formation of total aromatic compounds from the beginning of the post-oxidation zone. The concentration profile remains constant in the post-oxidation zone, and its value is comparable to the final concentration of soot that has been experimentally determined. Consequently, it has been hypothesized that the amount of carbonaceous species, which contributes to soot formation, is already present at the flame front in the form of high-molecular-mass structures. This result excludes the massive contribution of a surface growth mechanism to the soot loading, in slightly sooting regimes.

It is now important to understand if this picture of particulate formation can be applied also to aromatic fuel flames, which have a higher propensity to form soot.

In this paper, we use the developed kinetic mechanism^{16–18} to simulate fuel-rich, low-pressure, premixed benzene/oxygen flames. The comparison is performed with flames that have been well-characterized, in terms of gaseous products and high-molecular-mass aromatics, i.e., the Bittner and Howard flame at an equivalence ratio of $\Phi = 1.8$ ¹⁹ and the McKinnon flame ($\Phi = 2.4$),²⁰ which recently has been characterized by Grieco et al.⁴

The results obtained for the benzene flames are then compared with those obtained in an ethylene flame, studied by Ciajolo et al.,³ to determine the differences and similarities in the processes of aromatic growth and soot formation.

Flame Model and Mechanism

The kinetic model that describes the high-temperature oxidation of benzene includes Emdee et al.²¹ and Frank et al.²² submechanisms, with improvements by Zhang and McKinnon.²³ We have also used some of the

elementary reactions from the Wang and Frenklach benzene oxidation mechanism.⁹

The chemical kinetic mechanism of light hydrocarbons includes a modified version of Miller and Melius's gas kinetic model.²⁴ Miller²⁵ subsequently included the reactions $i\text{-C}_4\text{H}_5 + \text{H} \leftrightarrow \text{C}_3\text{H}_3 + \text{CH}_3$, $i\text{-C}_4\text{H}_5 + \text{H} \leftrightarrow \text{CH}_3\text{-CCCH}_2 + \text{H}$, and $\text{CH}_3\text{CCCH}_2 + \text{H} \leftrightarrow \text{C}_3\text{H}_3 + \text{CH}_3$ to account for the production of C_3H_3 and 1-methylallenyl radicals. This modified version of the Miller and Melius light hydrocarbons/fix gas kinetic model is used as the basis upon which to build a detailed growth chemistry of hydrocarbons.

Three routes for the formation of phenyl radical and benzene are included in the reaction mechanism. The first is the addition of $n\text{-C}_4\text{H}_3$ ($\text{HC}\equiv\text{C}-\text{CH}=\text{CH}$) to C_2H_2 , leading to phenyl (R197), and, similarly, the addition of $n\text{-C}_4\text{H}_5$ ($\text{H}_2\text{C}=\text{CH}-\text{CH}=\text{CH}$) to C_2H_2 , leading to benzene + H (R196). The rate coefficients of these reactions are adapted from Wang and Frenklach's Rice–Ramsperger–Kassel–Marcus (RRKM) calculations.⁹ The second route is the self-combination of propargyl radicals by $\text{H}_2\text{CCCH} + \text{H}_2\text{CCCH} \leftrightarrow \text{C}_6\text{H}_5 + \text{H}$ (R191) and also by $\text{H}_2\text{CCCH} + \text{C}_3\text{H}_2 \leftrightarrow \text{C}_6\text{H}_5$ (R192). The aforementioned reactions cannot be considered as single-step reactions, because not only the initial adduct, but also several of the rearrangement intermediates are aliphatic C_6 -species, which transform to either fulvene, benzene, or phenyl + H. An overall rate constant of $3 \times 10^{12} \text{ cm}^3 \text{ mol}^{-1} \text{ s}^{-1}$ is assigned to these reactions, in reasonably agreement with the measured rate constants^{26,27} and those derived by modeling benzene concentrations measured in premixed flames.^{24,28–31} The last sequence forming benzene involves 1-methylallenyl and propargyl combining to form benzyl radicals and their decomposition to benzene (R203). A rate constant of $3 \times 10^{12} \text{ cm}^3 \text{ mol}^{-1} \text{ s}^{-1}$ is assigned to benzyl formation.

The kinetic sub-mechanism for the formation of larger aromatic structures include either the replicating hydrogen abstraction carbon addition (HACA) mechanism, or kinetic pathways involving resonantly stabilized free radicals. The HACA mechanism occurs by way of a two-step process involving hydrogen abstraction to activate aromatics, followed by subsequent acetylene addition.³² This process continues, leading to the sequential formation of multi-ring structures (such as naphthalene, phenanthrene, and higher-order rings). Byproducts of the process are ethynyl-substituted PAH and five-membered aromatics such as acenaphthylene. The rate constants proposed by Wang and Frenklach⁹ are used.

Four different reaction sequences of resonantly stabilized radicals, which are potentially important sources for PAH growth, are analyzed. Dean³³ suggested the

(13) Tregrossi, A.; Ciajolo, A.; Barbella, R. *Combust. Flame* **1999**, *117* (3), 553–561.

(14) Seinfeld, J. H.; Pandis, S. N. *Atmospheric Chemistry and Physics: From Air Pollution to Climate Change*; Wiley: New York, 1998.

(15) D'Anna, A.; Violi, A.; D'Alessio, A.; Sarofim, A. F. *Combust. Flame* **2001**, *127* (1–2), 1995–2003.

(16) D'Anna, A.; Violi, A. *Proc. Combust. Inst.* **1998**, *27*, 425.

(17) Violi, A.; D'Anna, A.; D'Alessio, A. *Chem. Eng. Sci.* **1999**, *54*, 3439.

(18) D'Anna, A.; Violi, A.; D'Alessio, A. *Combust. Flame* **2000**, *121* (3), 418–429.

(19) Bittner, J. D.; Howard, J. B. *Proc. Combust. Inst.* **1981**, *18*, 1105.

(20) McKinnon, J. Th.; Howard, J. B. *Proc. Combust. Inst.* **1992**, *24*, 965.

(21) Emdee, J.; Brezinsky, K.; Glassman, I. *J. Phys. Chem.* **1992**, *96*, 2151.

(22) Frank, P.; Herzler, J.; Just, Th.; Wahl, C. *Proc. Combust. Inst.* **1994**, *25*, 833.

(23) Zhang, H.-Y.; McKinnon, J. T. *Combust. Sci. Technol.* **1995**, *107*, 261.

(24) Miller, J. A.; Melius, C. F. *Combust. Flame* **1992**, *91* (1), 21–39.

(25) Miller, J. A. *Proc. Combust. Inst.* **1996**, *26*, 461.

(26) Alkamade, U.; Homann, K. H. *Z. Phys. Chem. Neue Folge* **1989**, *161*, 19–34.

(27) Westmoreland, P. R.; Dean, A. M.; Howard, J. B.; Longwell, J. P. *J. Phys. Chem.* **1989**, *93*, 8171.

(28) Stein, S. E.; Walker, J. A.; Suryan, M. M.; Fahr, A. *Proc. Combust. Inst.* **1990**, *23*, 85.

(29) Morter, C. L.; Farhat, S. K.; Adamson, J. D.; Glass, G. P.; Curl, R. F. *J. Phys. Chem.* **1994**, *98*, 7029.

(30) Atkinson, D. B.; Hudgens, J. W. *J. Phys. Chem.* **1999**, *103*, 4242.

(31) Pope, Ch. J.; Miller, J. A. *Proc. Combust. Inst.* **2000**, *28*, 1519.

(32) Frenklach, M.; Wang, H. *Proc. Combust. Inst.* **1991**, *23*, 1559.

(33) Dean, A. M. *J. Phys. Chem.* **1990**, *94*, 1432.

combination of two resonantly stabilized cyclopentadienyl radicals to form naphthalene. Subsequently, Marinov et al.¹¹ and Melius et al.³⁴ proposed the same reaction sequence but with 2H as products (R247) using a rate constant of $2 \times 10^{13} \exp[-8000/(RT)] \text{ cm}^3 \text{ mol}^{-1} \text{ s}^{-1}$. Although this reaction has a reasonably high activation energy, it is considered, in the present analysis, to be a temperature-independent rate, to overcome the controversy on the value of the activation energy. The range of temperatures in both the flames analyzed is comparable; consequently, the differences in the activation energy will not affect model conclusions. In this work, a rate constant of $3 \times 10^{11} \text{ cm}^3 \text{ mol}^{-1} \text{ s}^{-1}$ is assigned to R247. The value used for R247 is ~ 10 times higher than that proposed by Dean³³ but significantly lower than that used by Marinov et al.¹¹ and Melius et al.³⁴ It is instead in reasonable agreement with that derived by modeling benzene flames by the MIT group.¹² However, the value proposed ensures a reasonable good agreement between predictions and experiments in both benzene and ethylene flames analyzed in this work.

Colket and Seery³⁵ proposed reactions involving the resonantly stabilized benzyl radicals forming PAH. Specifically, the key PAH formation step is the combination of benzyl and propargyl, yielding naphthalene, for which they proposed a rate constant of $6.02 \times 10^{11} \text{ cm}^3 \text{ mol}^{-1} \text{ s}^{-1}$. In this work, a rate constant of $3 \times 10^{11} \text{ cm}^3 \text{ mol}^{-1} \text{ s}^{-1}$ is assigned to this reaction (R242).

The formation of phenanthrene by reaction of phenyl radicals with benzene, forming biphenyl, and subsequent acetylene addition is also considered (R365). The rate constants for this path are evaluated following Wang and Frenklach.⁹

The computations were performed using the Sandia laminar one-dimensional premixed flame code (PREMIX) of the Chemkin package.³⁶ The PREMIX code computes the species profiles for a burner-stabilized premixed laminar flame, using the cold mass flow rate through the burner, feed-gas composition, pressure, and an estimated solution profile as input. The program can also compute the temperature profile. However, heat losses to the burner surface and the external environment are unknown; therefore, an experimentally determined temperature profile is used as input.

Thermochemical information was primarily obtained from the Chemkin thermodynamic database,³⁶ from Stein et al.,²⁸ and from Marinov et al.¹¹ Unavailable thermodynamic properties for some species were estimated using Benson's group additivity method.³⁷ The transport parameters were obtained from the Chemkin database³⁶ and from Wang and Frenklach.³⁸

The reaction mechanism consists of 492 reactions and 105 chemical species. Unless specifically mentioned, each elementary reaction in the mechanism is revers-

ible. The reverse reaction rates were calculated using equilibrium constants. For most of the recombination and decomposition reactions, the pressure dependence in the Troe format and third-body efficiencies were taken into consideration.³⁹

The reactions of the aromatic growth sub-mechanism are listed for convenience in Table 1, where they are cited with their original source.

Experimental Data

To test the capability of the kinetic mechanism to model the oxidation of benzene and the growth of aromatics, experimental data that were reported by the MIT group were used for comparison.^{2,4,19,20}

Bittner and Howard analyzed a low-pressure premixed benzene/oxygen/argon flame.¹⁹ The 2.63 kPa flame was supported on a cooled copper plate burner that had been drilled with 1-mm-diameter holes. The feed composition was 13.5 mol % benzene, 56.5 mol % oxygen, and 30.0 mol % argon at a cold gas velocity of 50 cm/s (at 298 K). The equivalence ratio was $\Phi = 1.8$, corresponding to a "nearly sooting" condition. Using a molecular beam/mass spectrometer, the authors were able to measure the profiles of small radicals and stable species; temperatures were measured using radiation-corrected thermocouples. In the following text, this flame will be referenced as Flame I.

The second set of experimental data is represented by the concentration profiles of stable gaseous species and condensable material collected in a premixed low-pressure benzene/oxygen/argon flame stabilized on a water-cooled burner and equipped with a sampling system for direct product collection. The flame, here called Flame II, was operated at a fuel equivalence ratio of $\Phi = 2.4$, a cold gas velocity of $v = 25 \text{ cm/s}$, a pressure of $P = 5.33 \text{ kPa}$ and a fraction of argon in fuel mixture of 10 mol %. The condensable material was fractionated in soot, fullerenes, and high-molecular-mass aromatics.^{2,4,20}

Finally, experimental data on soot and condensable material collected by Ciajolo et al.³ in a rich sooting ethylene/air flame at atmospheric pressure were used for comparison with benzene flames. This flame, named Flame III, was stabilized on a McKenna burner at a fuel equivalence ratio of $\Phi = 2.4$, a cold gas velocity of $v = 4 \text{ cm/s}$, and a pressure of $P = 100 \text{ kPa}$. Table 2 summarizes the operating conditions of the flames analyzed.

Model Results

Modeling the growth of big PAH and the formation of particulate matter requires reasonably good predictions for stable species, small intermediates, and key radical species such as H and OH. Such capability of the new kinetic mechanism is shown in Figure 1, where model predictions for C_6H_6 , O_2 , CO , CO_2 (Figure 1a), H_2 , H_2O (Figure 1b), and H and OH (Figure 1c) are compared with experimental data for Flame I. The experimental temperature profile used as input for flame modeling is reported in Figure 1a as a dashed line.

Reactants and combustion products (Figure 1a) are predicted quite well: the benzene and oxygen concentrations rapidly decrease in the flame zone, which is located $\sim 1.0 \text{ cm}$ above the burner, where the flame temperature reaches its maximum value ($\sim 1900 \text{ K}$). The formation of carbon monoxide, which is a major product in rich combustion, also occurs in the flame zone,

(34) Melius, C. F.; Colvin, M. E.; Marinov, N. M.; Pitz, W. J.; Senkan, S. M. *Proc. Combust. Inst.* **1996**, *26*, 685.

(35) Colket, M. B.; Seery, D. J. *Proc. Combust. Inst.* **1994**, *25*, 883.

(36) Kee, R. J.; Rupley, F. M.; Miller, J. A.; Coltrin, M. E.; Grcar, J. F.; Meeks, E.; Moffat, H. K.; Lutz, A. E.; Dixon-Lewis, G.; Smooke, M. D.; Warnatz, J.; Evans, G. H.; Larson, R. S.; Mitchell, R. E.; Petzold, L. R.; Reynolds, W. C.; Caracotsios, M.; Stewart, W. E.; Glarborg, P. CHEMKIN Collection, Release 3.5, Reaction Design, Inc., San Diego, CA, 1999.

(37) Benson, S. W. *Thermochemical Kinetics*, Second Edition; Wiley: New York, 1976.

(38) Wang, H.; Frenklach, M. *Combust. Flame* **1994**, *96*, 163–170.

(39) Troe, J. *Ber. Bunsen-Ges. Phys. Chem.* **1983**, *87*, 161–169.

Table 1. Aromatic Growth Submechanisms

submechanism	reaction	$K = AT^n \exp[-E_a/(RT)]$			reference/comment
		A ($\text{cm}^3 \text{mol}^{-1} \text{s}^{-1} \text{K}^{-n}$)	n	E_a (cal/mol)	
Benzene Oxidation					
R207	$\text{C}_6\text{H}_6 + \text{O}_2 = \text{C}_6\text{H}_5 + \text{HO}_2$	6.3×10^{13}		60000	Zhang and McKinnon ²³
R232	$\text{C}_6\text{H}_6 + \text{OH} = \text{C}_6\text{H}_5\text{OH} + \text{H}$	1.3×10^{13}		10994	Frank et al. ²²
R234	$\text{C}_6\text{H}_6 + \text{O} = \text{C}_6\text{H}_5 + \text{OH}$	1.0×10^1	3.8	1790	Frank et al. ²²
R231	$\text{C}_6\text{H}_6 + \text{H} = \text{C}_6\text{H}_5 + \text{H}_2$	2.5×10^{14}		16005	Wang and Frenklach ⁹
R233	$\text{C}_6\text{H}_6 + \text{OH} = \text{C}_6\text{H}_5 + \text{H}_2\text{O}$	2.1×10^{13}		4569	Wang and Frenklach ⁹
R235	$\text{C}_6\text{H}_6 + \text{O} = \text{C}_6\text{H}_5\text{OH}$	2.2×10^{13}		4530	Frank et al. ²²
R392	$\text{C}_6\text{H}_6 + \text{O} = \text{C}_6\text{H}_5\text{O} + \text{H}$	2.2×10^{13}		4530	Emdee et al. ²¹
R398	$\text{C}_6\text{H}_5\text{O} + \text{O} \rightarrow \text{HCO} + 2\text{C}_2\text{H}_2 + \text{CO}$	3.0×10^{13}			Emdee et al. ²¹
R229	$\text{C}_6\text{H}_5\text{O} + \text{H} = \text{C}_6\text{H}_5\text{OH}$	2.5×10^{14}			Emdee et al. ²¹
R396	$\text{C}_6\text{H}_5\text{O} \rightarrow \text{C}_5\text{H}_5 + \text{CO}$	1.5×10^{12}		43853	Frank et al. ²²
R397	$\text{C}_6\text{H}_5\text{O} + \text{H} \rightarrow \text{C}_5\text{H}_6 + \text{CO}$	3.0×10^{13}			Frank et al. ²²
R236	$\text{C}_6\text{H}_5\text{OH} + \text{H} = \text{C}_6\text{H}_5\text{O} + \text{H}_2$	2.3×10^{14}		12404	Frank et al. ²²
R237	$\text{C}_6\text{H}_5\text{OH} + \text{O} = \text{C}_6\text{H}_5\text{O} + \text{OH}$	1.3×10^{13}		2891	Frank et al. ²²
R238	$\text{C}_6\text{H}_5\text{OH} + \text{OH} = \text{C}_6\text{H}_5\text{O} + \text{H}_2\text{O}$	1.0×10^{13}			Frank et al. ²²
R210	$\text{C}_6\text{H}_5 + \text{O}_2 = 2\text{CO} + \text{C}_2\text{H}_2 + \text{C}_2\text{H}_3$	7.5×10^{13}		15002	Zhang and McKinnon ²³
R211	$\text{C}_6\text{H}_5 + \text{OH} = \text{C}_6\text{H}_5\text{O} + \text{H}$	5.0×10^{13}			Emdee et al. ²¹
R221	$\text{C}_6\text{H}_5 + \text{O}_2 = \text{C}_6\text{H}_5\text{O} + \text{O}$	1.0×10^{13}		6120	Frank et al. ²²
R223	$\text{C}_6\text{H}_5 + \text{O} \rightarrow \text{C}_5\text{H}_5 + \text{CO}$	2.0×10^{14}			Frank et al. ²²
R417	$\text{C}_5\text{H}_4\text{O} \rightarrow \text{CO} + 2\text{C}_2\text{H}_2$	1.0×10^{15}		78000	Emdee et al. ²¹
R216	$\text{C}_5\text{H}_6 + \text{H} = \text{C}_5\text{H}_5 + \text{H}_2$	2.2×10^8	1.8	3000	Frank et al. ²²
R217	$\text{C}_5\text{H}_6 + \text{O} = \text{C}_5\text{H}_5 + \text{OH}$	1.8×10^{13}		3080	Frank et al. ²²
R219	$\text{C}_5\text{H}_6 + \text{O}_2 = \text{C}_5\text{H}_5 + \text{HO}_2$	2.0×10^{13}		25000	Frank et al. ²²
R218	$\text{C}_5\text{H}_6 + \text{OH} = \text{C}_5\text{H}_5 + \text{H}_2\text{O}$	3.4×10^9	1.18	-447	Zhang and McKinnon ²³
R187	$\text{C}_5\text{H}_6 + \text{H} \rightarrow \text{CH}_2\text{CHCH}_2 + \text{C}_2\text{H}_2$	1.0×10^{13}		12000	Zhang and McKinnon ²³
R404	$\text{C}_5\text{H}_5 + \text{H} = \text{C}_5\text{H}_6$	1.0×10^{14}			Frank et al. ²²
R188	$\text{C}_5\text{H}_5 + \text{O} \rightarrow \text{CH}_2\text{CHCHCH} + \text{CO}$	1.0×10^{14}			Castaldi et al. ¹⁰
R189	$\text{C}_5\text{H}_5 + \text{O} = \text{C}_5\text{H}_4\text{O} + \text{H}$	3.0×10^{13}			Castaldi et al. ¹⁰
R190	$\text{C}_5\text{H}_5 + \text{OH} = \text{C}_5\text{H}_4\text{OH} + \text{H}$	3.0×10^{13}			Emdee et al. ²¹
R407	$\text{C}_5\text{H}_5 + \text{HO}_2 = \text{C}_5\text{H}_5\text{O} + \text{OH}$	1.0×10^{12}			Emdee et al. ²¹
R411	$\text{C}_5\text{H}_5\text{O} \rightarrow \text{CH}_2\text{CHCHCH} + \text{CO}$	2.5×10^{11}		43900	Emdee et al. ²¹
R412	$\text{C}_5\text{H}_5\text{O} + \text{H} \rightarrow \text{CH}_2\text{O} + 2\text{C}_2\text{H}_2$	3.0×10^{13}			estimated
R413	$\text{C}_5\text{H}_5\text{O} + \text{O} \rightarrow \text{CO}_2 + \text{CH}_2\text{CHCHCH}$	3.0×10^{13}			estimated
R414	$\text{C}_5\text{H}_4\text{OH} = \text{C}_5\text{H}_4\text{O} + \text{H}$	2.1×10^{13}		48000	Emdee et al. ²¹
R415	$\text{C}_5\text{H}_4\text{OH} + \text{H} \rightarrow \text{CH}_2\text{O} + 2\text{C}_2\text{H}_2$	3.0×10^{13}			Emdee et al. ²¹
R416	$\text{C}_5\text{H}_4\text{OH} + \text{O} \rightarrow \text{CO}_2 + \text{CH}_2\text{CHCHCH}$	3.0×10^{13}			Emdee et al. ²¹
R417	$\text{C}_5\text{H}_4\text{O} \rightarrow \text{CO} + 2\text{C}_2\text{H}_2$	1.0×10^{15}		78000	Emdee et al. ²¹
R418	$\text{C}_5\text{H}_4\text{O} + \text{O} \rightarrow \text{CO}_2 + 2\text{C}_2\text{H}_2$	3.0×10^{13}			estimated
Benzene Formation					
R191	$\text{C}_3\text{H}_3 + \text{C}_3\text{H}_3 = \text{C}_6\text{H}_5 + \text{H}$	3.0×10^{12}			Miller and Melius ²⁴
R192	$\text{C}_3\text{H}_3 + \text{C}_3\text{H}_2 = \text{C}_6\text{H}_5$	3.0×10^{12}			Miller and Melius ²⁴
R196	$n\text{C}_4\text{H}_5 + \text{C}_2\text{H}_2 = \text{C}_6\text{H}_6 + \text{H}$	1.0×10^{16}	-1.33	5400	Wang and Frenklach ⁹
R197	$n\text{C}_4\text{H}_3 + \text{C}_2\text{H}_2 = \text{C}_6\text{H}_5$	2.8×10^3	+2.90	1400	Wang and Frenklach ⁹
R203	$\text{C}_4\text{H}_5 + \text{C}_3\text{H}_3 = \text{C}_6\text{H}_5\text{CH}_2 + \text{H}$	3.0×10^{12}			Castaldi et al. ¹⁰
R204	$\text{C}_6\text{H}_5 + \text{CH}_3 = \text{C}_6\text{H}_5\text{CH}_2 + \text{H}$	5.7×10^{-2}	5	15700	Zhang and McKinnon ²³
R206	$\text{C}_6\text{H}_5\text{CH}_3 + \text{H} = \text{C}_6\text{H}_6 + \text{CH}_3$	1.2×10^{13}		5148	Zhang and McKinnon ²³
Aromatic Growth					
R242	$\text{C}_6\text{H}_5\text{CH}_2 + \text{C}_3\text{H}_3 = \text{C}_{10}\text{H}_8 + 2\text{H}$	3.0×10^{11}			estimated
R365	$\text{C}_6\text{H}_5\text{C}_6\text{H}_4 + \text{C}_2\text{H}_2 = \text{C}_{14}\text{H}_{10} + \text{H}$	6.6×10^{33}	-5.92	22600	Wang and Frenklach ⁹
R247	$\text{C}_5\text{H}_5 + \text{C}_5\text{H}_5 = \text{C}_{10}\text{H}_8 + 2\text{H}$	3.0×10^{11}			estimated
R334	$\text{C}_{10}\text{H}_7 + \text{C}_2\text{H}_2 = \text{C}_{12}\text{H}_8 + \text{H}$	6.6×10^{33}	-5.92	22600	Wang and Frenklach ⁹
R250	$\text{C}_9\text{H}_7 + \text{C}_5\text{H}_5 = \text{C}_{14}\text{H}_{10} + 2\text{H}$	3.0×10^{11}			estimated
R284	$\text{C}_6\text{H}_5 + \text{C}_2\text{H}_2 = \text{C}_6\text{H}_5\text{C}_2\text{H} + \text{H}$	5.1×10^{38}	-7.09	29600	Wang and Frenklach ⁹
R287	$\text{C}_6\text{H}_5\text{C}_2\text{H} + \text{H} = \text{C}_6\text{H}_4\text{C}_2\text{H} + \text{H}_2$	2.5×10^{14}		16000	Wang and Frenklach ⁹
R313	$\text{C}_6\text{H}_4\text{C}_2\text{H} + \text{C}_2\text{H}_2 = \text{C}_{10}\text{H}_7$	1.4×10^{51}	-11.58	26000	Wang and Frenklach ⁹
Aromatic Oxidation					
R455	$\text{C}_{10}\text{H}_7 + \text{O}_2 \rightarrow \text{C}_6\text{H}_5\text{C}_2\text{H} + \text{HCO} + \text{CO}$	2.0×10^{12}		7488	Wang and Frenklach ⁹
R460	$\text{C}_{12}\text{H}_7 + \text{O}_2 \rightarrow \text{C}_{10}\text{H}_7 + 2\text{CO}$	2.0×10^{12}		7488	Wang and Frenklach ⁹
R427	$\text{C}_{10}\text{H}_8 + \text{OH} \rightarrow \text{C}_6\text{H}_5\text{C}_2\text{H} + \text{CH}_3\text{CO}$	1.0×10^{11}			Wang and Frenklach ⁹
R430	$\text{C}_{12}\text{H}_8 + \text{OH} \rightarrow \text{C}_{10}\text{H}_8 + \text{HCCO}$	1.0×10^{11}			Wang and Frenklach ⁹
R460	$\text{C}_{14}\text{H}_{10} + \text{OH} \rightarrow \text{C}_{10}\text{H}_7\text{C}_2\text{H} + \text{CH}_3\text{CO}$	1.0×10^{11}			Wang and Frenklach ⁹

Table 2. Hydrocarbon/Oxygen/Argon Flames

	Value		
	flame I	flame II	flame III
hydrocarbon	benzene	benzene	ethylene
argon content (%)	30	10	0
equivalence ratio, Φ	1.8	2.4	2.4
pressure, P (kPa)	2.67	5.33	100
maximum temp, T_{max} (K)	1900	1900	1750
cold gas velocity, v (cm/s)	50	25	4
reference	19	2, 4	3

corresponding to the consumption of the fuel and oxidant. CO subsequently oxidizes to CO_2 and both CO

and CO_2 concentrations slowly increase, remaining quite constant in the post-flame zone. The same behavior is also shown by the profile of H_2O and H_2 (Figure 1b), except for a small decrease of H_2O concentration in the post-oxidation zone of the flame, which is reasonably captured by the kinetic model. The reaction mechanism also reproduces the values and trends of OH and H concentrations (see Figure 1c).

The consumption channels of benzene are primarily reactions with H, OH, and O atoms forming phenyl radicals by H-atom abstraction. Oxygen can also be added to the aromatic ring, forming phenoxy, cyclo-

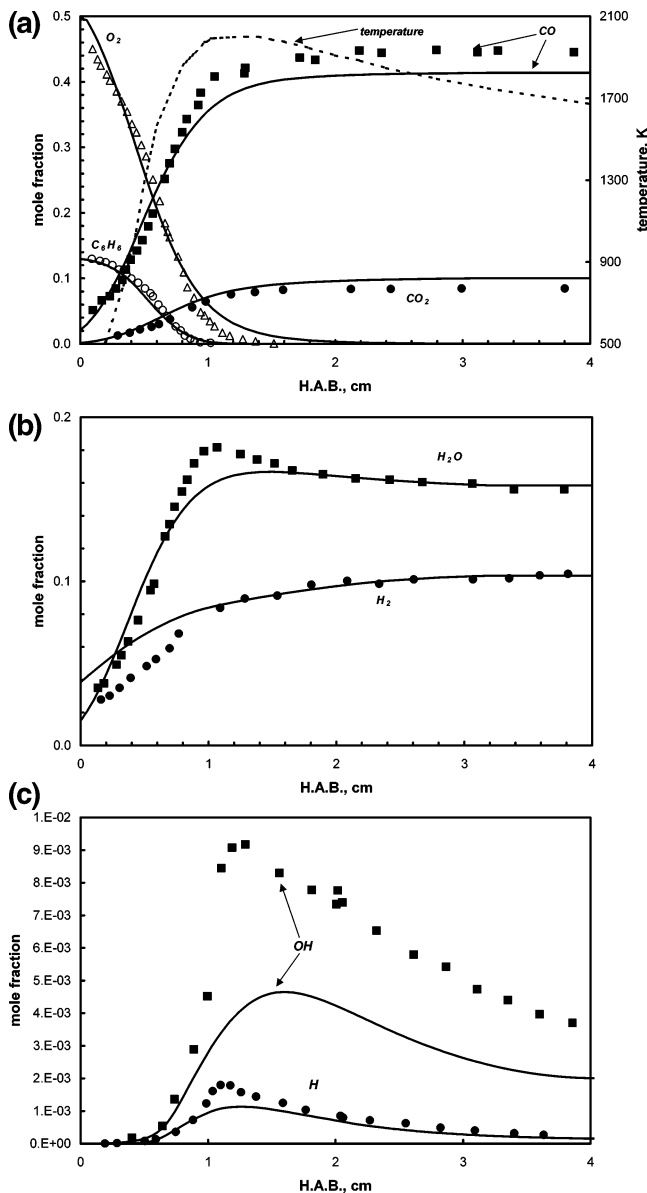


Figure 1. Comparison between experimental mole fraction profiles (symbols)¹⁹ and model predictions (solid lines) in a nearly sooting benzene/oxygen flame (Flame I): (a) C₆H₆, O₂, CO, and CO₂; (b) H₂ and H₂O; and (c) H and OH. The experimental temperature profile is shown as a dashed line in Figure 1a.

pentadienyl radicals, and CO:

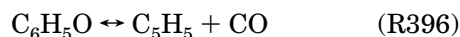
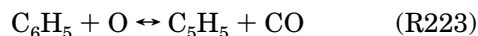
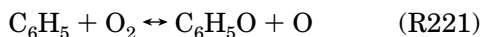


Figure 2 reports the comparison between predicted and experimental concentration profiles of phenyl (C₆H₅), cyclopentadienyl (C₅H₅), phenol (C₆H₅OH), and cyclopentadiene (C₅H₆), which are the main products of benzene oxidation that retain the ring structure. The model predicts quite well the concentration trends of both radical and stable species, except for a shift of the model predictions of ~1 mm toward the burner in the simulation of the phenyl radical.

Phenoxy (R396) and cyclopentadienyl (R188) radicals are then oxidized by O atoms, producing CO and light

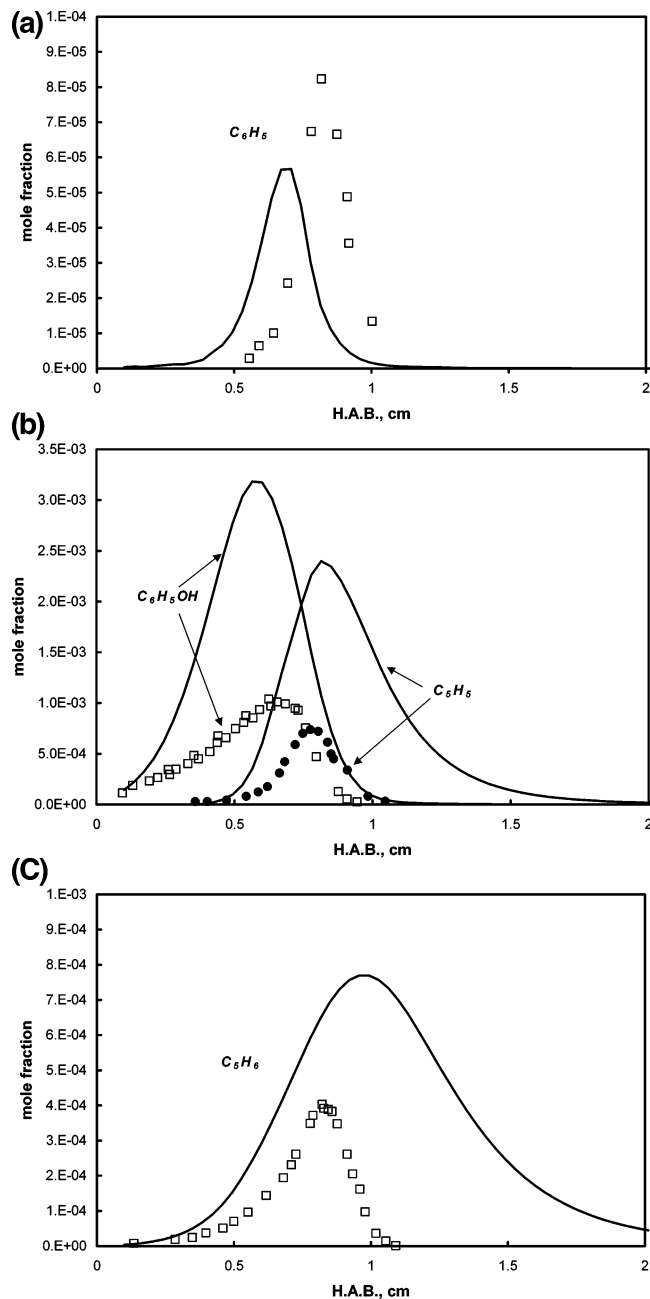


Figure 2. Comparison between experimental mole fraction profiles (symbols)¹⁹ and model predictions (solid lines) in a nearly sooting benzene/oxygen flame (Flame I): (a) phenyl (C₆H₅), (b) cyclopentadienyl (C₅H₅) and phenol (C₆H₅OH), and (c) cyclopentadiene (C₅H₆).

hydrocarbons. However, the phenyl radical can also react with H atoms, forming benzene (in this way, the net aromatic consumption is zero), or with C₂H₂, forming phenylacetylene (R284), which starts the molecular growth process. Phenyl may also decompose, forming C₃ + C₃ and C₄ + C₂.

Figure 3 reports the comparison of the predicted and experimental concentration profiles of methyl and propargyl radicals and phenylacetylene. Figure 4 shows the concentration profiles of acetylene, methane, and ethane. The model is able to reproduce their profiles in the first part of the flame well, up to the maximum value; however, it does not predict their decay for heights greater than 1 cm above the burner. The model properly computes the maximum values of CH₄ and C₂H₆,

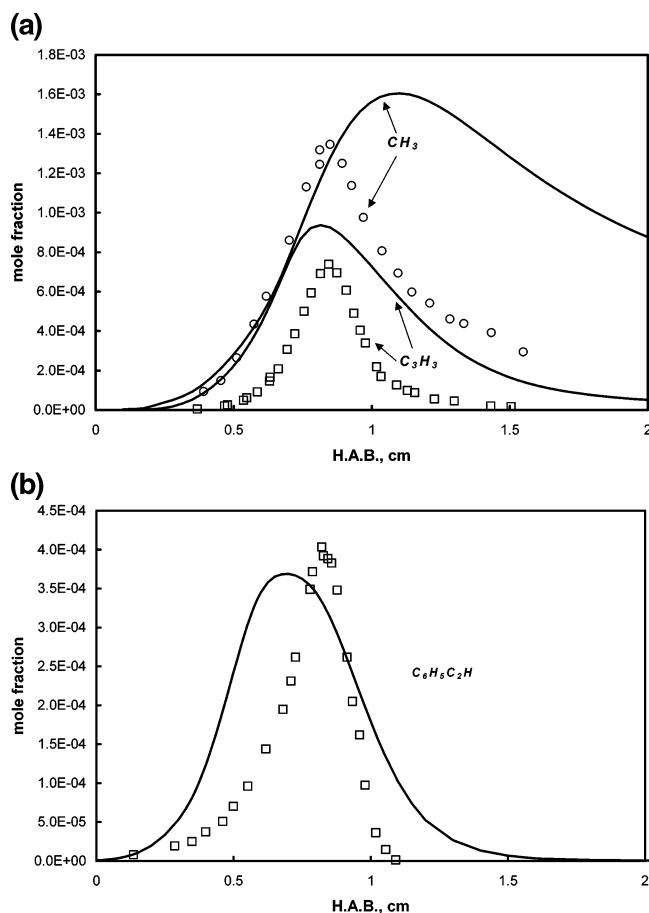


Figure 3. Comparison between experimental mole fraction profiles (symbols) and model predictions (solid lines) in a nearly sooting benzene/oxygen flame (Flame I): (a) CH_3 (methyl) and C_3H_3 (propargyl), and (b) $\text{C}_6\text{H}_5\text{C}_2\text{H}$ (phenylacetylene).¹⁹

whereas the acetylene maximum concentration is within a factor of 2.

The good agreement of the computed profiles of stable species and free radicals with experimental data is a rigorous test of the model capability to reproduce also aromatic fuel flames, and it is essential for the confident application of the model to larger species and the assessment of potential errors and uncertainties.

Several PAH were identified by Bittner and Howard in their study of the near-sooting benzene flame. Because the kinetic mechanism is unable, at the present stage, to describe the detailed distribution of the high-molecular-mass pyrolytic carbon, a direct comparison of PAH mole fraction predictions with experimental data is not possible. However, the comparison with experimental data can be performed with the total aromatic hydrocarbons collected in flames, i.e., the concentration of all the species with a mass of 200 a.u. and bigger.

Figure 5 shows the comparison between the predicted concentration of total aromatic hydrocarbons with more than two rings and the measured signal from species larger than 200 a.u. The experimental concentration is reported on an arbitrary unit scale, because Bittner and Howard did not perform any calibration of their spectrometric signal. Consequently, the comparison may be done only with the shape of the two concentration curves. The two profiles show the same behaviors: a rapid increase of the concentration, which maximizes

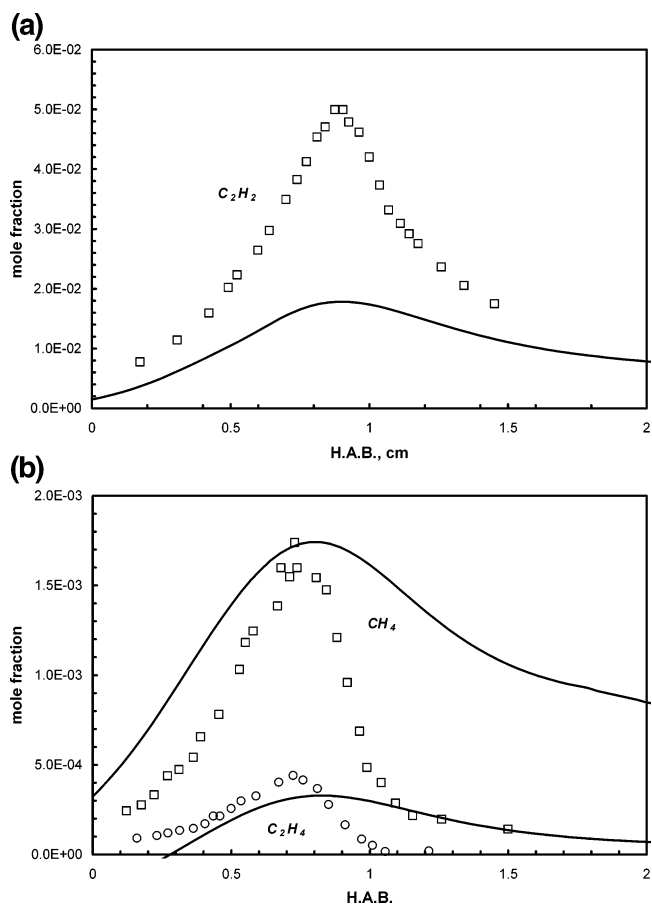


Figure 4. Comparison between experimental mole fraction profiles (symbols) and model predictions (solid lines) in a nearly sooting benzene/oxygen flame (Flame I): (a) C_2H_2 and (b) CH_4 and C_2H_4 .¹⁹

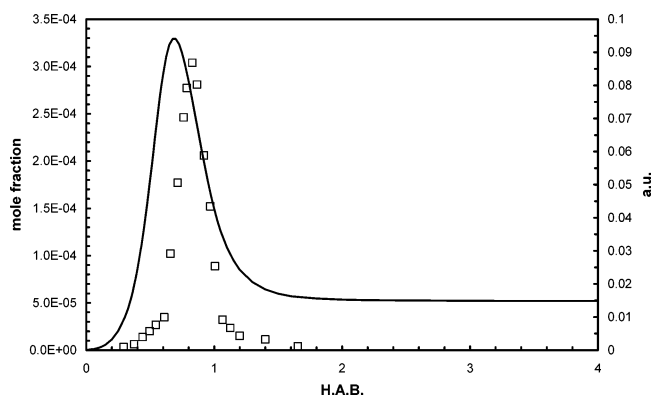


Figure 5. Computed mole fraction profiles of total aromatic species (molecular masses larger than naphthalene), compared with the signal of species larger than 200 a.u.¹⁹ in a nearly sooting benzene/oxygen flame (Flame I). Symbols denote experimental data, and solid line represents the computed profile.

at ~ 8.5 mm, followed by a decrease of the species concentration across the end of the main oxidation zone (~ 1 cm). These observations are consistent with a fast formation of PAH in the main flame region, which react among themselves, growing in size. Thereafter, they are rapidly consumed at the flame front by the pyrolysis and oxidative pyrolysis of the high-molecular-mass species.

The concentration of high-molecular-mass aromatics has been also measured by the MIT group in Flame

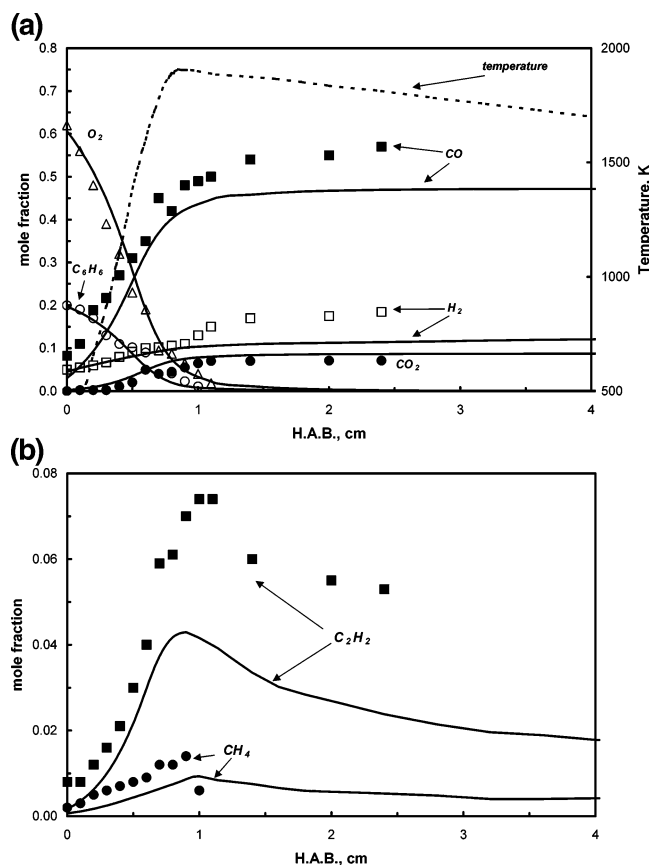


Figure 6. Comparison between experimental mole fraction profiles (symbols) and model predictions (solid lines) in a sooting benzene/oxygen flame (Flame II): (a) C_6H_6 , O_2 , CO , CO_2 , and H_2 ; and (b) C_2H_2 and CH_4 .^{2,4} The experimental temperature profile is shown as a dashed line in Figure 6a.

II.^{2,4,20} The model predicts the concentration profiles of stable species in this new benzene flame reasonably well, as shown in Figure 6, for C_6H_6 , O_2 , CO , CO_2 , H_2 (Figure 6a), CH_4 , and C_2H_2 (Figure 6b), when compared with the experimental data. The mechanism also reproduces both the value and the trend of total particulate carbon collected in flame, i.e., the concentration of dichloromethane-soluble material and soot. This comparison is reported in Figure 7, where the two sets of measurements performed by McKinnon² and Grieco et al.⁴ (symbols) on the same flame are reported. The concentration of total particulate peaks before the end of the main oxidation zone, then decreases across the maximum temperature zone and levels off with distance from the burner, attaining the soot concentration profile, which represents the major fraction of the total particulate carbon in the post-oxidation zone of the flame. The same behavior is also shown by the computed profile: a buildup of aromatic compounds in the main flame zone, and their decomposition in the high-temperature region of the flame.

The agreement between the model result and the total amount of particulate carbon collected in flame shows that the formation of two- and three-ring aromatics (which are the high-molecular-mass compounds included in the kinetic scheme) is the rate-determining step in the formation of total organic carbon. The concentration of these compounds gives the possibility to predict the final concentration of soot and high-molecular-mass aromatics also in benzene flames.

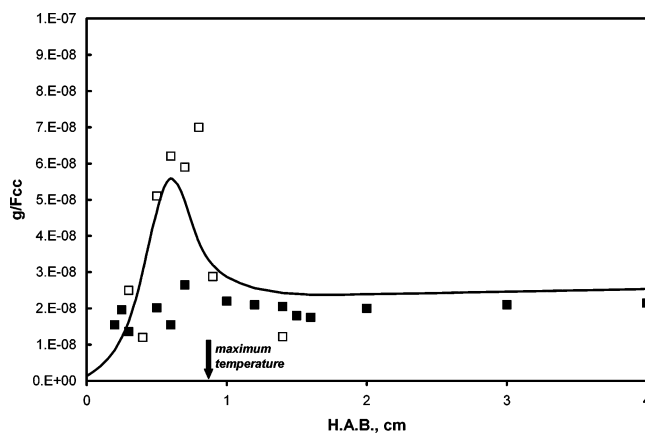


Figure 7. Experimental (symbols: (□) McKinnon² and (■) Grieco et al.⁴) and computed (solid line) concentration profiles (given in g/cm^3 under flame conditions) of total particulate in a sooting benzene/oxygen/argon flame with an equivalence ratio of $\Phi = 2.4$ (Flame II).^{2,4} (Model predictions are for total species larger than naphthalene.)

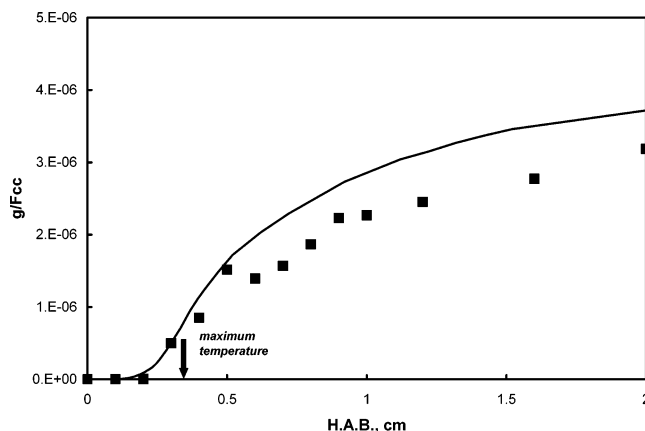


Figure 8. Experimental (symbols) and computed (solid line) concentration profiles of total particulate in a sooting ethylene/oxygen flame with an equivalence ratio of $\Phi = 2.4$ (Flame III).³

Here, the different behaviors of high-molecular-mass compounds in aromatic and aliphatic flames are analyzed by comparing the results obtained for the benzene flame with those obtained in an ethylene flame experimentally studied by Ciajolo et al. (Flame III). Experimental data were obtained through sampling and chemical analysis. As reported elsewhere,^{16–18} the model predicts the concentration profiles of stable species in this ethylene flame reasonably well.

Figure 8 reports the concentration profiles of total aromatic compounds in the ethylene flame, compared with experimental data. The buildup of aromatics in the ethylene flame occurs just at the flame front, and their concentration reaches a constant value in the post-oxidation region. The model is able to reproduce the total amount and concentration profile of these species correctly.

Discussion

The mechanism identifies two main pathways in rich combustion. The first pathway is the hydrocarbon oxidation, in which the main products are C_2 and C_1 fragments, CO , and CO_2 . The other pathway is the molecular growth, with the building-up of species with a molecular mass higher than that of the starting hydrocarbon.

The pathway for ethylene oxidation includes the direct attack of OH atoms to the ethylene molecules, leading to the formation of ketene and subsequent decomposition to CO and the H-atom abstraction from the ethylene molecule with the formation of vinyl radicals. The latter radicals are then oxidized by OH to CO, which is subsequently only partially oxidized to CO₂, because of the lack of OH radicals in rich combustion. Vinyl radicals also undergo reactions such as dehydrogenation and decomposition, which lead to the formation of acetylene and methyl radicals, respectively. These reactions are more important when few OH radicals are available for the fuel oxidation, resulting in a large formation of C₂H₂ and CH₄. Vinyl radicals also undergo combination reactions, forming pyrolytic species that have more than two C atoms. The combination of vinyl radicals with methyl leads to the formation of C₃ species and, by successive H-atom abstraction, to the formation of the resonantly stabilized propargyl radicals (C₃H₃), which reach relatively high concentrations in flame, because of their stability. The combination of vinyl radicals with acetylene produces C₄ species such as *n*-C₄H₅. However, these radicals are present in low concentrations, because they are easily converted in the more-stable isomers *i*-C₄H₅, whose concentration in flames is relatively high.

The reactions of these resonantly stabilized radicals are the main source of benzene in flames. Self-combination of propargyl radicals and the addition of C₂H₂ to *i*-C₄H₅ account for ca. 90% of benzene production, with the remaining contribution being due to the addition of propargyl to 1-methylallenyl radicals; the latter also are present at high concentrations in flames. The contribution of C₂H₂ addition to *n*-C₄H₅ and *n*-C₄H₃ radicals is negligible under high-temperature conditions.

Hence, benzene formation is the rate-limiting step for aromatic growth in the ethylene flame and it is formed across the flame front. Carbon growth continues through the formation of multi-ring aromatics, which are formed through the H-atom abstraction and acetylene addition mechanism and through the propargyl addition to benzyl radicals and the cyclopentadienyl self-combination. The routes that involve the resonantly stabilized radicals are the dominant ones in the main oxidation zone, because of the large formation of *c*-C₅H₅ and benzyl radicals from benzene and toluene oxidation.

Unlike the ethylene flame, in the benzene oxidation, the aromatic ring is already present in the oxidation zone and it is mainly oxidized to *c*-C₅H₅ radicals. As a consequence, differently from the ethylene oxidation zone, a large amount of cyclopentadienyl radicals is immediately available for recombination reactions, leading to multi-ring aromatic formation. This occurs already below the flame front, where large amounts of aromatics are formed. The increase of temperature at the flame front reduces their concentration, because of pyrolysis and/or oxidation, resulting in a peak value in the main oxidation region and a leveling-off in the post-

oxidation zone of the flame. Cyclopentadienyl self-combination is the dominant route in the multi-ring aromatic formation process, whereas benzyl and propargyl combination is less important and contributes mainly in the post-flame region. The H-atom abstraction and acetylene addition mechanism is of minor importance in the entire flame region.

In the benzene flame, the aromatic growth and oxidation processes are concurrent. The building blocks for larger aromatic formation are the main products of benzene oxidation, so that larger aromatics are formed in the main oxidation zone of the flame.⁴⁰

Conclusions

A new detailed kinetic model has been developed that is able to predict, with a reasonable level of accuracy, smaller species and key radical species, as well as the concentration profiles of total aromatics in aromatic and aliphatic flames.

The model considers the role of resonantly stabilized radicals in the growth of aromatic species, in addition to the HACA mechanism, which involves H-atom abstraction to activate aromatics, followed by subsequent acetylene addition.

From this study, it results that the self-combination of resonantly stabilized radicals is the controlling pathway of aromatic ring growth. In particular, the combination of cyclopentadienyl radicals is the dominant route of multi-ring aromatic formation.

In ethylene flames, cyclopentadienyl radicals are formed behind the flame through oxidation of benzene that is formed by the molecular growth of ethylene. Larger aromatic hydrocarbons build-up in the post-oxidation zone of the flame with a fast formation rate, attaining an almost-constant value in the post-flame region.

In the oxidation of benzene fuel, the aromatic ring is already present in the main oxidation zone, and it is mainly oxidized to *c*-C₅H₅ radicals. As a consequence, a large amount of cyclopentadienyl radicals are available for recombination reactions during the main oxidation process, leading to multi-ring aromatic formation already below the flame front. The high temperature of the flame zone, which favors decomposition and/or oxidation of the larger aromatics, leads to an almost-constant concentration of these species downstream of the flame zone.

The model reproduces the experimental trends, and, more importantly, it is able to identify the two different behaviors for aliphatic and aromatic flames. In particular, in benzene flames, the reaction mechanism reproduces the decrease in the particulate concentration profile within the flame front, which has been observed experimentally but never predicted numerically.

EF0499675

(40) Richter, H.; Howard, J. B. *Prog. Energy Combust. Sci.* **2000**, *26*, 565.